European Polymer Journal 44 (2008) 1978–1987

Contents lists available at ScienceDirect

European Polymer Journal

journal homepage: www.elsevier.com/locate/europolj

Macromolecular Nanotechnology

Structure and properties of an hybrid system based on bisphenol A polycarbonate modified by A polyamide 6/organoclay nanocomposite

I. Goitisolo, J.I. Eguiazábal *, J. Nazabal

Departamento de Ciencia y Tecnología de Polímeros and Instituto de Materiales Poliméricos "POLYMAT", Facultad de Ciencias Químicas UPV/EHU, Paseo Manuel Lardizábal 3, 20018 San Sebastián, Spain

ARTICLE INFO

Article history:
Received 25 January 2008
Received in revised form 4 April 2008
Accepted 18 April 2008
Available online 25 April 2008

Keywords:
Fibrillation
Hybrid nanocomposites
Polyamide 6
Polycarbonate

ABSTRACT

Blends of poly(carbonate of bisphenol A) (PC) with minute amounts of a nanocomposite based in polyamide 6 (PA6) with a layered organoclay (nPA6) were obtained upon melt mixing by varying the contents of both nPA6 and organoclay. The ternary nanocomposites (NC) were composed of a PC-rich matrix with some mixed PA6 present, and by a neat nPA6 dispersed phase. Upon dissolution of the matrix of the NC's, the dispersed phase showed a highly fibrillar morphology that resembled that of thermoplastic/liquid crystalline polymer (LCP) blends. The cryogenically fractured surfaces observed by SEM showed a very fine particle size that was attributed to the presence of PA6 in the matrix and indicated a low interfacial tension. The Young's modulus behaviour is proposed to be a consequence of the slight orientation of the PC-rich matrix and the highly fibrillated and oriented nPA6 dispersed phase. The important reinforcement effect of the dispersed phase is attributed to the additive effects of its large degree of orientation, and the reinforcing effect of the organoclay.

1. Introduction

The reinforcement of polymers with layered organically modified clays as montmorillonite (OMMT) has led to the availability of a new class of polymer materials: the polymer nanocomposites [1]. This has triggered their use in perhaps the most attractive research field in polymer materials which is polymer blending. In this way, polymeric nanocomposites have begun to be used as new components in blends with other polymers as second components; thus, linking the ability to improve the performance by both blending and adding nanoparticles. The study of these multicomponent (at least 3) materials is complex concerning mainly morphology, location of the nanoparticles and interactions between the components.

As in the case of two polymer components, blending of a polymer nanocomposite and a polymer produces a system that contains, besides the dispersed clay, either a single miscible polymeric system, or an immiscible system with two polymeric phases. In the latter case, either blends of a thermoplastic and a rubbery material, or of two thermoplastics are usually obtained.

The existence of miscible polymer blends has allowed one to obtain highly dispersed polymer nanocomposites in matrices where dispersion is otherwise difficult. For instance, the ability of PA6 to widely exfoliate the OMMT and its miscibility with polyamide 6.6 (PA6.6), have been used to produce a widely dispersed PA6.6 nanocomposite by mixing PA6.6 with a widely dispersed PA6/OMMT masterbatch [2]. A similar technique was also used in polypropylene (PP) using maleinized polypropylene (mPP) [3], in polyethylene (PE) using either maleinized polyethylene (mPE) or mPP [4,5] or ethylene-vinyl acetate copolymer (EVA) [6], and in poly(vinyl chloride) and styrene-acrylonitrile copolymer using poly(ε-caprolactone) [7,8].

Adequate blending of a polymer nanocomposite with a rubber material may lead to toughened nanocomposites. In these blends, the presence of the organoclay in the matrix makes the blend stiffer while preserving high toughness

* Corresponding author. Tel.: +34 943015447; fax: +34 943015270.
E-mail address: josei.eguiazabal@ehu.es (J.I. Eguiazábal).

0014-3057/$ - see front matter © 2008 Elsevier Ltd. All rights reserved.
doi:10.1016/j.eurpolymj.2008.04.028

values. This occurred in PA6 based nanocomposites by mixing PA6 with a maleated styrene-butylene-co-ethylene-styrene [9–12] as well as with ethylene-propylene-diene [13] and maleinized ethylene/propylene-based rubber (EPR) [14,15] leading to stiffer materials with notched impact strength values up to 20 times greater than that of the matrix. In the case of other thermoplastics as PA6.6, the increases in the impact strength were smaller [16]. They were very large (30 times the impact strength of the matrix) in the case of PP with maleinized poly(ethylene-octene) [17], but after addition of an unusually large rubber content (40%).

In the case of polymer nanocomposite/thermoplastic blends, several attractive possibilities may take place. One possibility is compatibilization of the blend that may occur either through the location of the organoclay in the interphase, thus changing the interfacial tension as in poly(butylene terephthalate) (PBT)/PE [18] and PA6/mPP NC's [19], or through the presence of dispersed clay platelets in the matrix that hinder/suppress the coalescence of the dispersed phase as in PA6/EPR [15], PA6/poly(phenylene oxide) (PPO) [20] and poly(ethyl methacrylate)/polystyrene (PS) [21] NC's. Although the OMMT may be present in both components [22], most often the nanocomposite forms the matrix. This occurred in PA6 with PP [23,24], mPP [24–26], PPO [20], and LCP [27], and also in PBT with LCP [28] and also with maleinized EVA depending on the processing sequence [29]. In other blends, the OMMT was located in both the matrix and the interphase as in poly(methyl methacrylate)/PS [30] and PA6/mPP [31] NC's. The location of the OMMT was not studied in PP/PS [32] and PBT/PE [33] NC's.

Among the polymer nanocomposite/thermoplastic systems, to our knowledge no system has a nanocomposite as the dispersed phase. However, this could lead to reinforcements of the dispersed phase that could challenge those obtained by the widely studied thermoplastic/LCP blends. In those materials, very large reinforcements occur thanks to the extreme ability of the LCPs to orient in the melt state and to their very high modulus. Their high price (often tenfold that of thermoplastics) is their greatest disadvantage.

Although the scientific and applied relevance of both PC and PA6 is not in doubt, the possibility of reinforcing PC by mixing it with a PA6 nanocomposite has not been studied to our knowledge. It is known that PA6 is able to widely exfoliate organoclays [34–36], and that exfoliation is difficult and only occurs to a minor extent in PC [37], where intercalation was the main result after melt blending [37,38]. The PC/PA6 blends were almost immiscible [39–41]. Interchange reactions could develop in the melt state, generally after a long processing time [40–43], leading to the presence of copolymers that should compatibilize the blends [40,42–44]. Adequate processing by injection moulding [39] may compatibilize the blends and produce a fibrillar dispersed PA6 phase that reinforces the PC. These characteristics of the blends will clearly change when one of the components is a nanocomposite. Among other changes at the polymer/OMMT interface, a decrease in the molecular mobility of chains may take place due to interactions [45], the presence of nanoreinforcements may hinder either the orientation of the dispersed phase [46,47] or a part of it [48], and the morphology of the whole dispersed phase could change as the viscosity of one phase is changed by the presence of OMMT.

In this work polymer nanocomposites based on blends of PC with small amounts of a PA6 based nanocomposite (previously prepared by melt mixing) have been obtained by direct injection moulding by changing both the nPA6 content of the blends and the OMMT content of the nPA6. The aim was to study: (i) the structure of the blends and relate it to the measured mechanical properties and (ii) the possibility of attaining reinforcement of the nPA6 dispersed phase (and, consequently, the ternary NC's) by the presence of OMMT and the possible orientation of this dispersed phase. PC/PA6 blends were used as a reference. The structure of the blends was studied by differential scanning calorimeter (DSC), dynamic-mechanical analysis (DMA) and scanning electron microscopy (SEM), as well as by density and melt flow index (MFI) measurements. The nanostructure was studied by transmission electron microscopy (TEM) and wide angle X-ray scattering (WAXS). The mechanical properties were measured by tensile tests.

2. Experimental

The PC used was Tarflon® lV1900R from Idemitsu Petrochemical Co. Ltd., and the PA6 was Durethan® B30S from Bayer. The filler was a montmorillonite (MMT) modified with octadecylammonium, Nanomer® I30TC, from Nanocor, Inc. (OMMT). Drying before processing was performed at 120 °C in an air-circulation oven for 12 h for PC, and at 80 °C in a dehumidifier for 12 h in the case of the PA6 or nPA6.

Nanocomposites based on PA6 (nPA6) were prepared by melt compounding PA6 with 2 wt% and 5 wt% OMMT in a Collin ZK25 co-rotating twin-screw extruder-kneader. The screws diameter and the L/D ratio were 25 mm and 30, respectively. The rotation speed was 200 rpm, and the die melt temperature 240 °C. The extrudates were cooled in a water bath and pelletized. The pellets were directly mixed and injection-moulded with PC to obtain ternary NC's in a Battenfeld BA-230E reciprocating screw injection moulding machine, and tensile (ASTM D638, type IV, thickness 1.84 mm) specimens. The screw of the plasticization unit was a standard screw with diameter of 18 mm, L/D ratio of 17.8 and compression ratio of 4. The melt temperature was 250 °C, and the mould temperature 15 °C. The injection speed and pressure were 23 cm^3/s and 1500 bar, respectively. PC/PA6 blends were also processed at the same conditions as a reference. The PA6 or nPA6 content varied from 0 to 50 wt%. A 75/25-2 NC refers to a NC with 75% PC, and 25% of a nPA6 that contains a 2% OMMT.

The phase structure was studied by DMA analysis performed using a TA Q800 that provided the loss tangent ($\tan\delta$) and the storage modulus (E') against temperature. A frequency of 1 Hz and a constant heating rate of 4 °C/min from −10 °C to 175 °C were used. The melting behaviour was studied by DSC using a Perkin-Elmer DSC-7 calorimeter. Indium was used as the reference material. The

samples were first heated from 30 °C up to 300 °C at 20 °C/min and then were cooled at the same rate. The melting temperature (T_m) and enthalpy (ΔH_m) were determined from the heating scan using the temperature of the maximum and the peak area, respectively. The crystallinity was calculated based on a melting heat of 190.6 J/g [49] for the 100% crystalline PA6. The crystallization temperature (T_c) was determined from the minimum of the exothermic peak in the cooling scan.

The specific volume of the blends was determined by the displacement method in a Mirage SD-120L electronic densitometer using butyl alcohol as immersion liquid. The estimated resolution was 0.003 cm^3/g. The MFI of the blends was measured with an ATS Faar extrusion plastometer at 250 °C and with a 2.16 kg load. Capillary extrusion measurements were performed at 250 °C in a Göttfert Rheograph 2002 rheometer using a flat entry capillary tungsten die with L/D ratio of 30/0.5.

Scanning electron microscopy (SEM) was carried out in a Hitachi S-2700 electron microscope on the core of gold coated cryogenically fractured tensile specimens at an accelerating voltage of 15 kV. SEM was also used to observe the dispersed PA6 phase after elimination of the PC phase introducing the central part of the injection-moulded specimens in 1,1,2,2,-tetrachloroethane for 24 h.

As the samples were not transparent, their orientation was measured using a Metricon Model 2010 equipped with an infrared laser with a wavelength of 1550 nm. The samples were prepared by sectioning the central part of the injected specimens in a Leica 1600 microtome.

X-ray diffraction patterns were recorded on a Philips PW 1729 GXRD X-ray diffractometer, operating at 45 kV and 50 mA, using a Ni-filtered CuKα radiation source. The scan speed was 0.5°/min. The transmission electron microscopy (TEM) samples were embedded in an epoxy resin and ultrathin-sectioned at 60–100 nm, using an ultramicrotome. The micrographs were obtained in a Hitachi 600AB apparatus at an accelerating voltage of 100 kV.

Tensile testing was carried out by using an Instron 4301 machine, at a crosshead speed of 10 mm/min and at 23 ± 2 °C and 50 ± 5% relative humidity. The mechanical properties (yield stress (σ_y) and ductility, measured as the break strain (ε_b)) were determined from the load–displacement curves. The Young's modulus was determined by means of an extensometer at a crosshead speed of 1 mm/min. A minimum of five tensile specimens were tested for each value reported.

3. Results and discussion

3.1. Phase behaviour

The composition dependence of the T_g's of the NC's as measured by DMA are shown in Fig. 1. As can be seen, despite the large PC content of the NC's, the low temperature T_g changed only slightly, indicating the presence of an almost pure PA6 phase. The small T_g decrease could be due to an enhanced motional amplitude of the amorphous chains [50] but also to a migration of the surfactant of the nPA6 that has been reported to occur [51,52]. The high

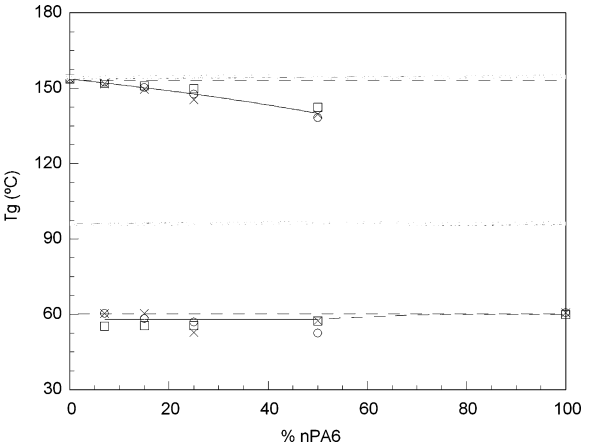

Fig. 1. T_g versus composition of the NC's, determined by DMA. (□) PC/nPA6-0, (○) PC/nPA6-2 and (×) PC/nPA6-5.

temperature T_g decreased, when the nPA6 content of the NC's increased. A similar decrease took place in the case of the blends without OMMT, indicating that there is a PC-rich phase present where some PA6 is dissolved. It can also be seen that the presence of OMMT did not change the position of the T_g's, and consequently the degree of miscibility of the blends.

This phase behaviour agrees with that previously observed in PC/PA6 blends [39–41]. The PA6 content in the PC-rich phase, calculated by means of the Fox equation [53], was roughly proportional to the PA6 content, reaching 10% in the 50/50 composition. Also, reactions may occur in PC/PA6 blends during processing [40–42]. However, it is expected that most of the PA6 in the PC-rich phase will be dissolved, since the change in T_g was small and the time in the melt state was short due to the direct injection moulding procedure employed.

The DSC results of the pure PA6 and of the NC's are shown in Fig. 2. As can be seen, the DSC results of the NC's were similar to those of the reference blends with the same PA6 content. The crystallization temperature of PA6 during cooling decreased. The decrease was the

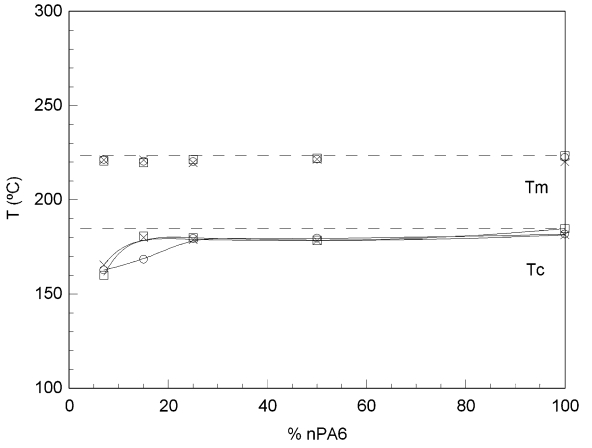

Fig. 2. T_c and T_m versus composition of the NC's, determined by DSC. Symbols as in Fig. 1.

maximum (25 °C) at the highest PC content, indicating that it hindered crystallization. The perfection of the crystals, however, did not change as the melting temperature was constant regardless of the PC or OMMT content. The crystalline content of the NC's increased linearly with PA6 content, indicating that the crystalline content of the pure PA6 (33%) did not change upon blending.

3.2. Nanostructure

The dispersion of the OMMT in the NC's was studied by both WAXS and TEM. The WAXS results of the NC's with 5% clay at different PA6 contents, as well as those of the reference OMMT are collected in Fig. 3. The results with smaller OMMT contents were similar. As can be seen, the peak of the OMMT at 3.65° (basal space: 2.42 nm) disappeared in the NC's. This suggests exfoliation, but does not rule out [54] the presence of either thin stacks or intercalated disordered nanostructures. The lack of diffraction peak also indicates the absence of agglomerated/collapsed clay layers (with repeating gallery distance) that may appear as a consequence of the additional processing required to mix the nPA6 with PC. It has been seen [55,56] that agglomeration of the clay layers in compact structures with interlayer distance smaller than the initial interlayer distance of the OMMT may occur upon harsh processing.

The nanostructure of the 93/7-5 and 50/50-2 NC's observed by TEM is shown, respectively in Fig. 4a and b. The rest of the NC's showed similar nanostructures. As can be seen in Fig. 4a, the OMMT present in the dispersed PA6 phase showed the typical, almost fully exfoliated nanostructure. With respect to the location of the OMMT upon mixing with PC, all the OMMT particles are occluded in the dispersed PA6-rich phase. This indicates that despite the small content of PA6, no migration to the majority PC-rich matrix occurred during blending. The OMMT was also only present in the PA6 phase in PA6/PP based NC's [19,57] but appeared in the PP phase when PP was modified with maleic anhydride [22]. The presence of OMMT in the dispersed PA6 phase of this study also agrees with the well-known, almost full "miscibility" of the OMMT in PA6 [35], especially when compared with the low compatibility between PC and the OMMT's [58].

In Fig. 4b (50/50-2 NC), the OMMT is in the PA6 matrix (as will be stated later) and the dispersed PC-rich phase is free of OMMT. No preferential location of the OMMT in the interphase is observed, which might occur, considering the presence of PA6 in the PC-rich phase. Moreover, no agglomeration of the OMMT layers was observed either in Fig. 4 or in the rest of the observed pictures.

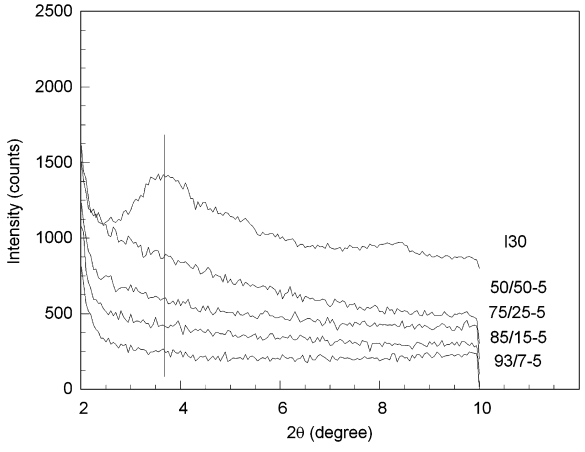

Fig. 3. WAXS patterns of the PC/nPA6-5 NC's at different nPA6 contents as well as that of the reference OMMT (I30).

3.3. Morphology

Upon inspection, the fractured tensile specimens showed a fibrillar morphology. This morphology is shown in Fig. 5 for the case of the ternary NC's with nPA-2. As it is seen, no fiber was macroscopically observed in the ternary NC's with 7% nPA6-2, but delamination in the skin and several thin fibers (not clearly seen in the photograph) appeared when the nPA6-2 content increased to 15%, and the fibrillar morphology was evident when the nPA6-2 content reached 25%. When specimens with different OMMT contents (not shown in Fig. 5) were compared, the observed fibrillation was similar, indicating that the fibrillation was roughly independent of the OMMT content.

To have additional information about the extent of the fibrillation, the matrix of the 85/15-2 NC was dissolved (see Section 2) exposing the nPA6 dispersed phase, that is shown in Fig. 6. As can be seen, nPA6 was present in the PC matrix as a very highly fibrillated and macroscopic (mostly above 0.1 mm length) structure. Similar fibers were observed at all nPA6 content. This fibrillation is a consequence of the tendency to fibrillate of the polyamides, and of the much higher viscosity of the PC matrix compared with that of the nPA6 dispersed phase, as will be seen later in this study. This high matrix viscosity leads to a very low viscosity ratio (η_d/η_m) value that favours fibrillation [27] of the dispersed phase; thus reinforcing the mechanical response of the NC's. These highly fibrillated morphologies and the fracture characteristics of Fig. 5 are very similar to those obtained in thermoplastic/LCP blends [59–61] indicating that similar reinforcements to those proper to the LCP's can be obtained with nPA6.

The morphology of the dispersed phase was studied by SEM in cryogenically fractured tensile specimens (Figs. 7 and 8). The effects of the OMMT content of the nPA6 phase are shown in Fig. 7. Fig. 7a shows the morphology of the 85/15-5 NC as an example, and Fig. 7b that of the reference 85/15 blend. Intermediate morphological characteristics were observed in the rest of the NC's. The morphology was similar throughout the cross section, and despite the previously observed fibrillar morphology, no skin phase structure, typical of thermoplastic/LCP blends appeared. As it is seen in Fig. 7a, the dispersed particle size is small and rather homogeneous, indicating that direct blending in the injection machine was effective enough. It is clear that the observed particles are not spherical, but are actually broken fibrils. Further, the particle size (typically 0.3 μm) was small, indicating that the interfacial tension

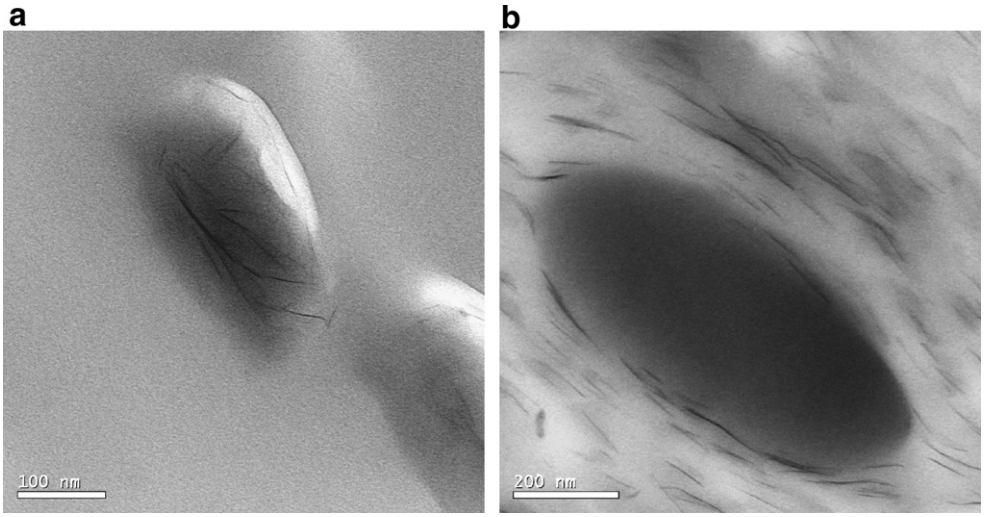

Fig. 4. TEM images of the 93/7-5 (a) and 50/50-2 (b) NC's.

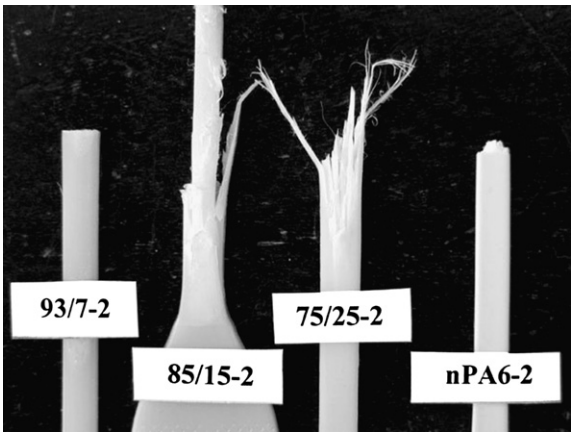

Fig. 5. Photograph of the fractured PC/nPA6-2 NC's tensile specimens.

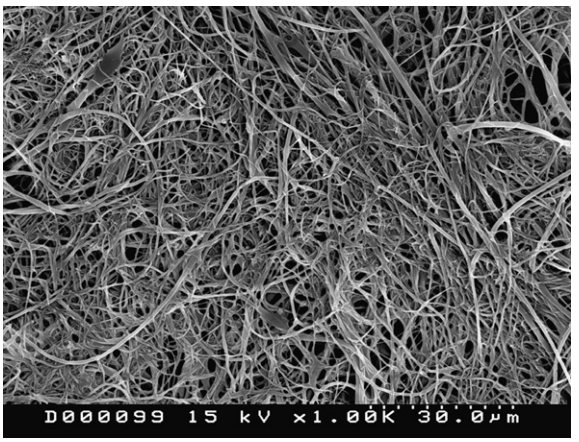

Fig. 6. SEM photomicrograph of the 85/15-2 dispersed phase after the extraction of the PC matrix.

in the melt state was low. This is attributed to the presence of some PA6 in the PC-rich phase.

Although some bigger particles appeared in the NC, the dispersed particle size of the reference blend (Fig. 7b) was rather similar to that of Fig. 7a. Phase coarsening upon OMMT addition was also observed in PP/nPA6 NC's [26]. This indicates that the presence of OMMT has only a slight effect on the particle size. Both increases [57] and decreases in viscosity were observed in PA6 [45,62,63] upon OMMT addition. This should influence the particle size. For this reason, the MFI's of the NC's of this study and those of the reference blends were measured and are shown in Fig. 9 as a function of composition. The sharp increase in MFI with the nPA6 content shows that the viscosities of both PA6 and nPA6 are clearly smaller than that of PC and that both of them behave as processing aids for PC. However, the curves of Fig. 9 are rather close to each other indicating that the change of MFI and viscosity with the OMMT content in the nPA6 was small. This small change of viscosity at the low shear rates typical of the MFI, agrees with the small change in particle size observed in Fig. 7 upon OMMT addition.

Fig. 8 shows the morphology of the NC's with 7, 15 and 25% nPA6-2 contents. The morphology of the 50/50-2 NC (not seen in Fig. 8) was close to co-continuity, with a matrix of the less viscous nPA6 and big PC-rich particles. The large dispersed particles occluded some smaller PA6 ones. Fig. 8 shows that the particle size increased with the nPA6 content, as expected. However, the increase in particle size was small. This is attributed to the fact that when the nPA6 content increases, the presence of PA6 in the PC-rich phase increases (the high temperature T_g decreased in Fig. 1). The presence of PA6 in the two phases lowers the interfacial tension in the melt state and, therefore, stabilizes finer morphologies. The presence of occluded particles inside the dispersed phase at large nPA6 contents, also agrees with a low interfacial tension in the melt.

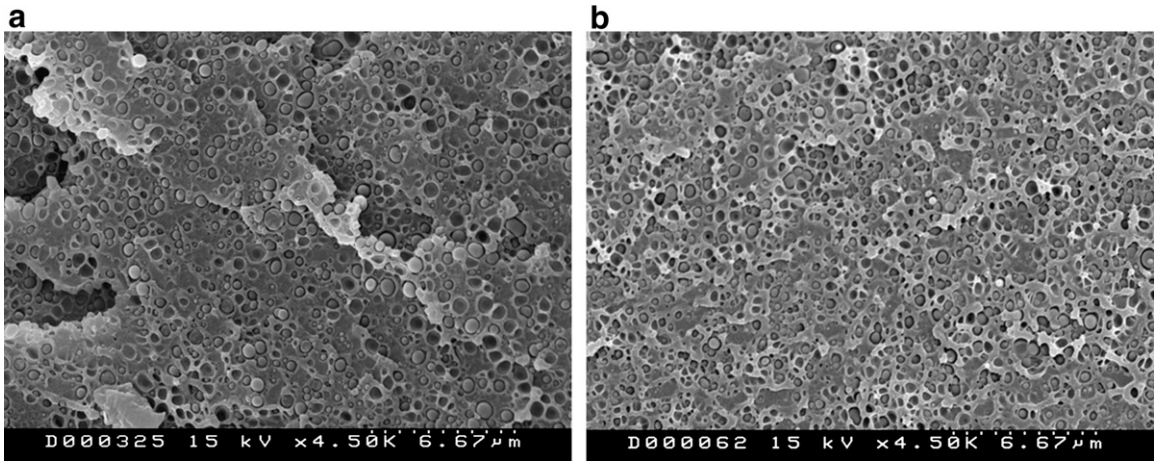

Fig. 7. SEM photomicrographs of the surfaces of cryogenically fractured NC's. (a) 85/15-5 and (b) 85/15-0.

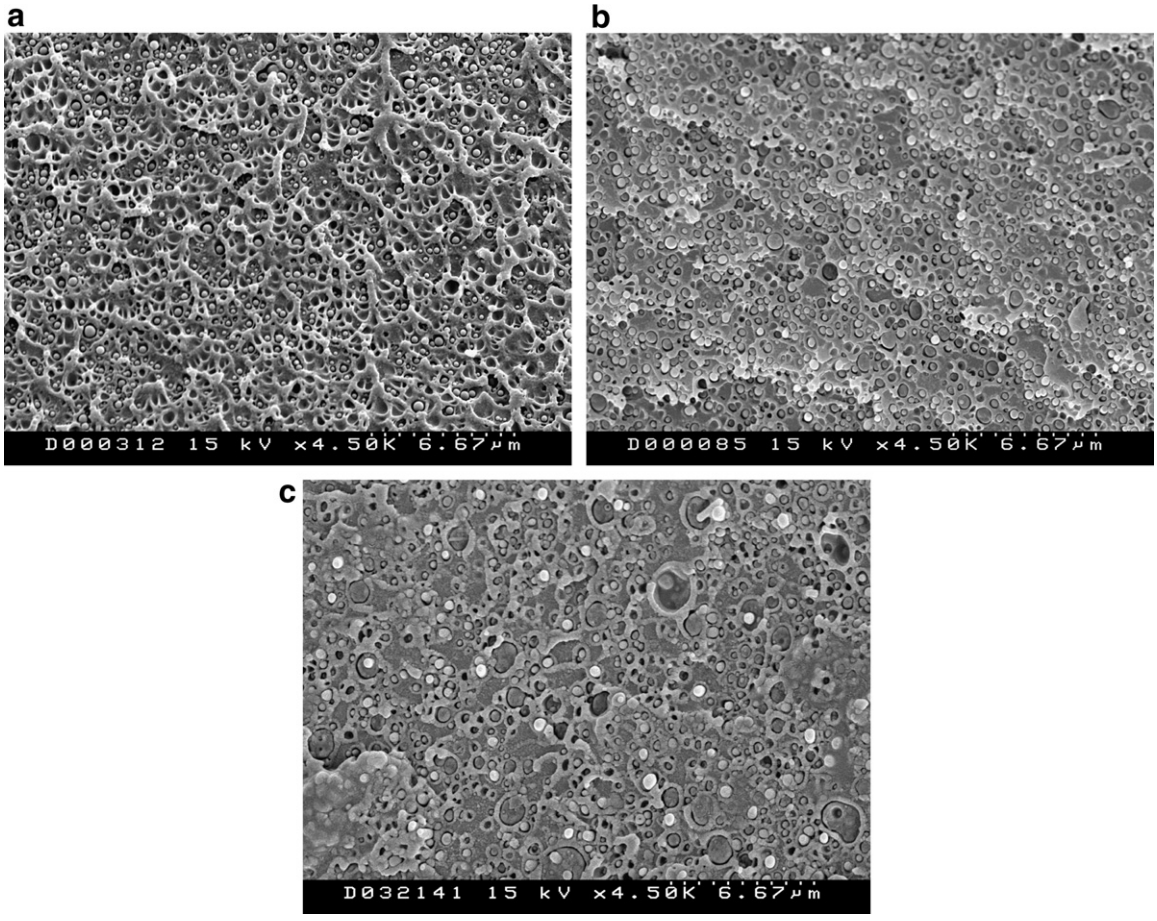

Fig. 8. SEM photomicrographs of the surfaces of cryogenically fractured NC's. (a) 93/7-2, (b) 85/15-2 and (c) 75/25-2.

3.4. Mechanical properties

The moduli of elasticity of the NC's and those of the reference blends are shown in Fig. 10 as a function of the nPA6 content. The broken linear lines are plotted as a reference. The plot of the yield stress was similar [63,64] although, as usual, the increase in magnitude was smaller. The increases in the moduli of the NC's with respect to the

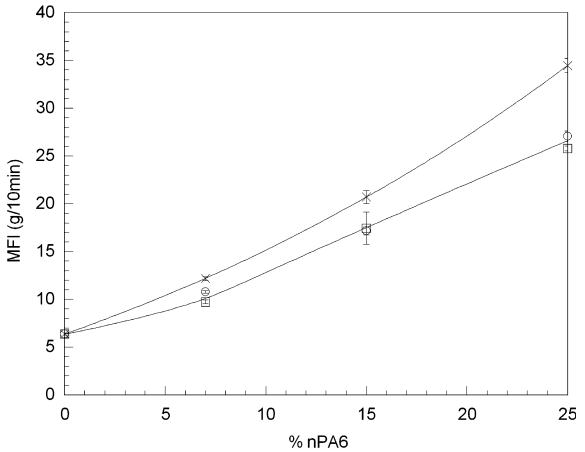

Fig. 9. MFI values of the NC's with nPA6-0 (□), nPA6-2 (○) and nPA6-5 (×) against composition.

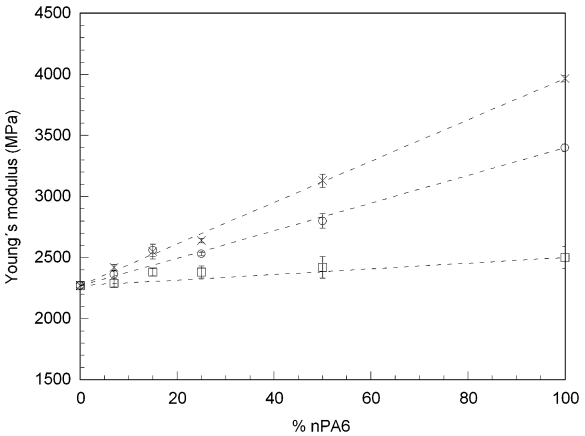

Fig. 10. Young's modulus of the NC's. Symbols as in Fig. 9.

neat blends are important. The increase was from 2.27 GPa to 2.56 GPa with only 15% nPA6-2 (OMMT content: 0.3%). These values are compared with those obtained in PC/LCP blends in Table 1. As can be seen, the increases in moduli of this study are even higher than those interpolated of LCP blends with the same reinforcing phase content. This is especially true at low contents, where the fibrillating ability of the LCP's is small.

One can propose two main factors that may give rise to the increase in modulus. The first factor is the presence of the oriented PA6 that leads to an increase in the modulus, as depicted by the slope of the plot of the reference blends. The second factor is the presence of OMMT that leads to an additional increase in the modulus which is depicted by the higher position of the modulus of the nPA6's with respect to that of the pure PA6 (see the vertical axis at the right). As the plots of the ternary NC's showed a behaviour with composition close to linearity, the orientation of the blends is preserved in the NC's, even though the presence of nanoreinforcements might hinder fibrillation [46]. Moreover, both the positive effects of the orientation and of the presence of OMMT are additive.

We now discuss the relationship between the NC morphology and the observed modulus behaviour. Besides the orientation, the main parameters that influence the modulus are the crystallinity and the specific volume. The crystallinity of the PA6 did not change upon blending, as observed before. The specific volume was linear with composition, indicating that the specific volume of the two components was the same in the neat polymers as in the blends. Therefore, neither of the two parameters influenced the modulus behaviour. The discussion on orientation will be made in the next section.

The ductility of the NC's measured by the elongation at break is shown in Fig. 11 versus the nPA6 content. As can be seen, the ductility values of the NC's are below the values of the blends, but they are relatively high taking into account their biphasic nature and that one of the components of the system is a nanocomposite. As the specific volume of the amorphous part of the NC's and the crystallinity did not change significantly with the OMMT content of the nPA6, the smaller ductility of the NC's is most probably due to the decrease in ductility of the dispersed nPA6 phase that has been seen to take place at increasing OMMT contents [34,63,64]. However, all the nPA6-2 and the 75/25-5 NC's, as well as the corresponding blends, yielded and were ductile; thus, demonstrating the compatible nature of these PC/nPA6 ternary systems. This is attributed to the aforementioned migration of PA6 to the PC phase during melt mixing, that decreases the interfacial tension in the interphase and compatibilizes the system.

3.5. Orientation of the polymeric phases

The orientation of the blends measured by laser birefringence is plotted in Fig. 12 against composition. It can be observed that the overall orientation was below what could be expected, considering the values of the pure components. This is in apparent contradiction with the behaviour close to linearity observed in the plot of the modulus, but the lack of proportionality between orientation and

Table 1
Percent increases in the modulus of PC/nPA6 NC's of this study compared with those of PC/LCP blends

System	Reference	nPA6 or LCP content					
		5	7	10	15	20	25
PC/nPA6-5	This work	–	7	–	13	–	17
PC/Vectra A	[66]	–	–	–	–	8	–
PC/Vectra A + 10% compat.		–	–	–	–	20	–
PC/synthesized LCP	[67]	4	–	6	–	14	–

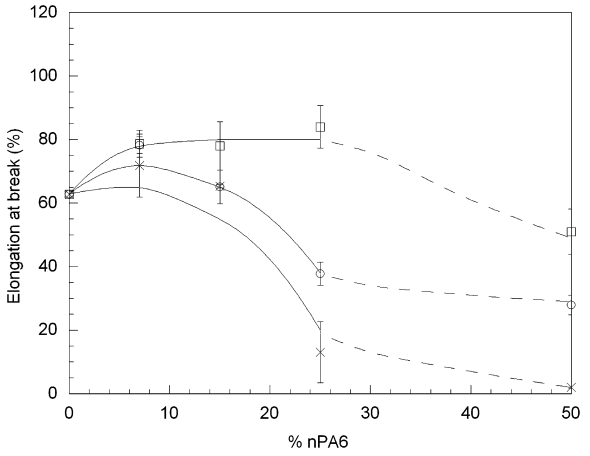

Fig. 11. Ductility measured as elongation at break of the NC's. Symbols as in Fig. 9.

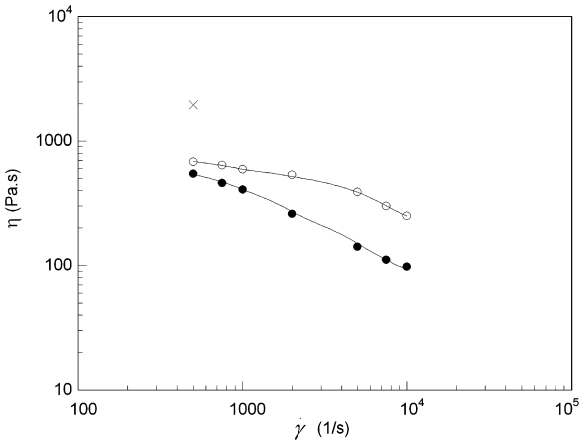

Fig. 13. Apparent viscosity of the pure PC (×) and of the 93/7-2 (○) and 93/7-5 (●) NC's as a function of the apparent shear rate.

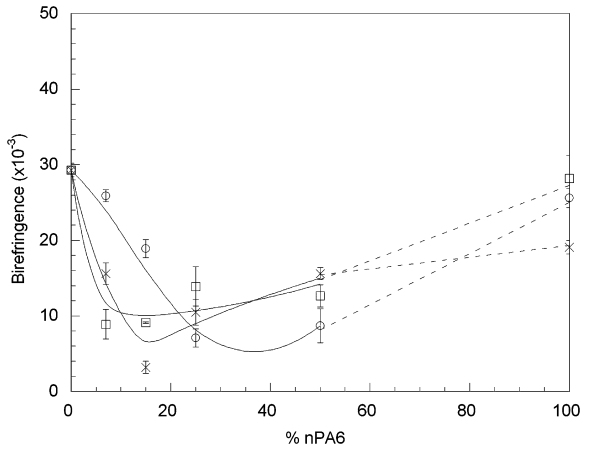

Fig. 12. The orientation of the NC's measured by laser birefringence. Symbols as in Fig. 9.

modulus at very different orientation levels [65], explains the different behaviour of the plot of the modulus and that of orientation of Fig. 12.

As can also be seen, the orientation of the whole blends strongly decreased upon nPA6 addition. This indicates a decrease in the orientation of the PC matrix when nPA6 is added, since it is clear that the dispersed phases are highly oriented (fibrillar morphology). This could be due to a decrease in viscosity [45,62,63]. To test whether this is the reason for the decrease in orientation of Fig. 12, the viscosity of the NC's with 7% nPA6 was measured and is plotted in Fig. 13. The viscosity of PC could be measured only at the lowest shear rate. As can be seen, the viscosity decreased upon addition of only 7% nPA6. This indicates an easier passage through the nozzle and the runner system that leads to a lower degree of orientation of the PC phase in the NC's compared with that of the neat state. Thus, in the observed modulus of elasticity (Fig. 10), the contribution of the nPA6 fibers is higher than what would be expected at those contents, particularly considering their large orientation. The contribution of the PC matrix, however, is less significant as a consequence of its low degree of orientation.

4. Conclusions

The PC/nPA6 ternary NC's are composed by an almost pure nPA6 phase and by a PC-rich phase, where some PA6 is dissolved. Neither the crystalline content, nor the perfection of the crystalline phase were modified upon blending. The OMMT was located in the dispersed nPA6 phase and its exfoliation level was very high and similar to that typical of the nPA6 neat systems.

The addition of nPA6 to PC led to an important viscosity decrease, and to extended fibrillation of the dispersed phase. Fibrillation during processing occurred regardless of nPA6 content, and thanks to both the high viscosity of the matrix, and to the tendency to fibrillate of the polyamides. The obtained fibers were very similar to those typical of blends reinforced with LCP's. The cryogenically fractured surfaces showed a small dispersed particle size that was attributed to the partial miscibility of the PA6 in the PC-rich matrix. The particle size was largely unchanged with the OMMT content of the nPA6, and changed only slightly at increasing nPA6 contents.

The increase in the modulus of elasticity was very high (from 2.27 GPa to 2.56 GPa with only 15% nPA6-2; i.e., with 0.3% OMMT). These high modulus values are attributed to two additive effects. These are, the reinforcement of the dispersed phase provided by its nanocomposite nature, and the reinforcement provided by the orientation/fibrillation of the dispersed nPA6-rich phase during injection moulding that was maintained in the NC's.

The observed modulus behaviour of the NC's was attributed to their degree of orientation, since the crystalline content of PA6 and the specific volume of the components did not change upon mixing. This orientation was relatively small in the PC-rich matrix, and large in the dispersed and fibrillated nPA6 phase.

Acknowledgements

The financial support of Spanish "Ministerio de Educación y Ciencia" (project number MAT2007-60153) is gratefully acknowledged. I. Goitisolo also acknowledges the Basque Government for the award of a grant for the development of this work.

References

[1] Bhattacharya SN, Gupta RK, Kamal MR. Polymeric nanocomposites. Munich: Hanser; 2008.
[2] González I, Eguiazábal JI, Nazabal J. Exfoliated PA6,6 nanocomposites by modification with PA6. Polymer 2005;46(9):2978–85.
[3] Gianelli W, Ferrara G, Camino G, Pellegatti G, Rosenthal J, Trombini RC. Effect of matrix features on polypropylene layered silicate nanocomposites. Polymer 2005;46(18):7037–46.
[4] Liang GD, Xu JT, Bao SP, Xu WB. Polyethylene maleic anhydride grafted polyethylene organic-montmorillonite nanocomposites. I. Preparation, microstructure and mechanical properties. J Appl Polym Sci 2004;91(6):3974–80.
[5] Lee J, Jung D, Hong C, Rhee K, Advani S. Properties of polyethylene-layered silicate nanocomposites prepared by melt intercalation with a PP-g-MA compatibilizer. Compos Sci Technol 2005;65: 1996–2002.
[6] Mainil M, Alexandre M, Monteverde F, Dubois P. Polyethylene organo-clay nanocomposites: the role of the interface chemistry on the extent of clay intercalation/exfoliation. J Nanosci Nanotechnol 2006;6(2):337–44.
[7] Lepoittevin B, Pantoustier N, Devalckenaere M, Alexandre M, Calberg C, Jerome R, et al. Polymer/layered silicate nanocomposites by combined intercalative polymerization and melt intercalation: a masterbatch process. Polymer 2003;44(7):2033–40.
[8] Kiersnowski A, Piglowski J. Polymer-layered silicate nanocomposites based on poly(epsilon-caprolactone). Eur Polym J 2004;40(6): 1199–207.
[9] González I, Eguiazábal JI, Nazabal J. Nanocomposites based on a polyamide 6/maleated styrene-butylene-co-ethylene-styrene blend: effects of clay loading on morphology and mechanical properties. Eur Polym J 2006;42(11):2905–13.
[10] González I, Eguiazábal JI, Nazabal J. Rubber-toughened polyamide 6/clay nanocomposites. Compos Sci Technol 2006;66(11–12):1833–43.
[11] González I, Eguiazábal JI, Nazabal J. Compatibilization level effects on the structure and mechanical properties of rubber-modified polyamide-6/clay nanocomposites. J Polym Sci Part B: Polym Phys 2005;43(24):3611–20.
[12] González I, Eguiazábal JI, Nazabal J. Effects of the processing sequence and critical interparticle distance in PA6-clay/mSEBS nanocomposites. Eur Polym J 2008;44(2):287–99.
[13] Wang K, Wang C, Li J, Su JX, Zhang Q, Du RN, et al. Effects of clay on phase morphology and mechanical properties in polyamide 6/EPDM-g-MA/organoclay ternary nanocomposites. Polymer 2007;48(7):2144–54.
[14] Ahn YC, Paul DR. Rubber toughening of nylon 6 nanocomposites. Polymer 2006;47(8):2830–8.
[15] Khatua BB, Lee DJ, Kim HY, Kim JK. Effect of organoclay platelets on morphology of nylon-6 and poly(ethylene-ran-propylene) rubber blends. Macromolecules 2004;37(7):2454–9.
[16] Dasari A, Yu ZZ, Mai YW. Effect of blending sequence on microstructure of ternary nanocomposites. Polymer 2005;46(16): 5986–91.
[17] Ma XY, Liang GZ, Lu HJ, Liu HL, Huang Y. Novel intercalated nanocomposites of polypropylene, organic rectorite, and poly(ethylene octene) elastomer: morphology and mechanical properties. J Appl Polym Sci 2005;97(5):1907–14.
[18] Hong JS, Namkung H, Ahn KH, Lee SJ, Kim C. The role of organically modified layered silicate in the breakup and coalescence of droplets in PBT/PE blends. Polymer 2006;47(11):3967–75.
[19] Chow WS, Mohd Ishak ZA, Karger-Kocsis J. Atomic force microscopy study on blend morphology and clay dispersion in polyamide-6/polypropylene/organoclay systems. J Polym Sci Part B: Polym Phys 2005;43:1198–204.
[20] Li YJ, Shimizu H. Novel morphologies of poly(phenylene oxide) (PPO)/polyamide 6 (PA6) blend nanocomposites. Polymer 2004;45(22):7381–8.
[21] Voulgaris D, Petridis D. Emulsifying effect of dimethyl-dioctadecy lammonium-hectorite in polystyrene/poly (ethylmethacrylate) blends. Polymer 2002;43(8):2213–8.
[22] Tang Y, Hu Y, Zhang R, Gui Z, Wang Z, Chen Z, et al. Investigation on polypropylene and polyamide-6 alloys/montmorillonite nanocomposites. Polymer 2004;45(15):5317–26.
[23] Chow WS, Mohd-Ishak ZA, Ishiaku US, Karger-Kocsis J, Apostolov AA. The effect of organoclay on the mechanical properties and morphology of injection-moulded polyamide 6/polypropylene nanocomposites. J Appl Polym Sci 2004;91(1):175–89.
[24] Chow WS, Abu Bakar A, Mohd Ishak ZA. Water absorption and hygrothermal aging study on organomontmorillonite reinforced polyamide 6/polypropylene nanocomposites. J Appl Polym Sci 2005;98(2):780–90.
[25] Chow WS, Mohd Ishak ZA, Karger-Kocsis J. Morphological and rheological properties of polyamide 6/poly(propylene)/organoclay nanocomposites. Macromol Mater Eng 2005;290(2):122–7.
[26] Gahleitner M, Kretzschmar B, Pospiech D, Ingolic E, Reichelt N, Bernreitner K. Morphology and mechanical properties of polypropylene/polyamide 6 nanocomposites prepared by a two-step melt-compounding process. J Appl Polym Sci 2006;100(1): 283–91.
[27] Zhang B, Ding Y, Chen P, Liu C, Zhang J, He J, et al. Fibrillation of thermotropic liquid crystalline polymer enhanced by nano-clay in nylon-6 matrix. Polymer 2005;46(14):5385–95.
[28] Chang IH, Seo BS, Kim SH. Blends of a thermotropic liquid-crystalline polymer and a poly(butylene terephthalate)/organoclay nanocomposite. J Polym Sci Part B: Polym Phys 2004;42(20): 3667–76.
[29] Li XC, Park HM, Lee JO, Ha CS. Effect of blending sequence on the microstructure and properties of PBT/EVA-g-MAH/organoclay ternary nanocomposites. Polym Eng Sci 2002;42(11):2156–64.
[30] Gelfer MY, Song HH, Liu LZ, Hsiao BS, Chu B, Rafailovich M, et al. Effects of organoclays on morphology and thermal and rheological properties of polystyrene and poly(methyl methacrylate) blends. J Polym Sci Part B: Polym Phys 2003;41(1):44–54.
[31] Chow WS, Mohd Ishak ZA, Karger-Kocsis J, Apostolov AA, Ishiaku US. Compatibilizing effect of maleated polypropylene on the mechanical properties and morphology of injection moulded polyamide 6/polypropylene/organoclay nanocomposites. Polymer 2003;44(24): 7427–40.
[32] Wang Y, Zhang Q, Fu Q. Compatibilization of immiscible poly(propylene)/polystyrene blends using clay. Macromol Rapid Commun 2003;24(3):231–5.
[33] Wu D, Zhou C, Zhang M. Effect of clay on immiscible morphology of poly(butylene terephthalate)/polyethylene blend nanocomposites. J Appl Polym Sci 2006;102(4):3628–33.
[34] Fornes TD, Hunter DL, Paul DR. Effect of sodium montmorillonite source on nylon 6/clay nanocomposites. Polymer 2004;45(7): 2321–31.
[35] Fornes TD, Yoon PJ, Hunter DL, Keskkula H, Paul DR. Effect of organoclay structure on nylon 6 nanocomposite morphology and properties. Polymer 2002;43(22):5915–33.
[36] Kim SW, Jo WH, Lee MS, Ko MB, Jho JY. Effects of shear on melt exfoliation of clay in preparation of nylon 6/organoclay nanocomposites. Polym J 2002;34(3):103–11.
[37] Hsieh AJ, Moy P, Beyer FL, Madison P, Napadensky E, Ren JX, et al. Mechanical response and rheological properties of polycarbonate layered-silicate nanocomposites. Polym Eng Sci 2004;44(5): 825–37.
[38] Yoon PJ, Hunter DL, Paul DR. Polycarbonate nanocomposites. Part 1. Effect of organoclay structure on morphology and properties. Polymer 2003;44(18):5323–39.
[39] Eguiazábal JI, Nazabal J. Compatibilization by processing and properties of polycarbonate/nylon 6 blends. Plast Rubber Process Appl 1990;14(4):211–7.
[40] Eguiazábal JI, Nazabal J. On the miscibility and interchange reactions in bisphenol A polycarbonate nylon 6 blends. Makromol Chemie-Macromol Symp 1988;20–21:255–67.
[41] Gattiglia E, Turturro A, Pedemonte E. Blends of polyamide-6 with bisphenol-A polycarbonate .1. Thermal-properties and compatibility aspects. J Appl Polym Sci 1989;38(10):1807–18.
[42] Gattiglia E, Turturro A, Lamantia FP, Valenza A. Blends of polyamide-6 and bisphenol-A polycarbonate – effects of interchange reactions on morphology and mechanical-properties. J Appl Polym Sci 1992;46(11):1887–97.
[43] Valenza A, Lamantia FP, Gattiglia E, Turturro A. Reactive blending of polyamide-6 and polycarbonate – effects of polyamide-6 terminal groups. Int Polym Proc 1994;9(3):240–5.

[44] Gattiglia E, Turturro A, Pedemonte E, Dondero G. Blends of polyamide 6 with bisphenol-A polycarbonate. 2. Morphology-mechanical properties relationships. J Appl Polym Sci 1990;41(7–8):1411–23.
[45] Alberola ND, Mele P. Interface and mechanical coupling effects in model particulate composites. Polym Eng Sci 1997;37(10):1712–21.
[46] Zhang XQ, Yang MS, Zhao Y, Zhang SM, Dong X, Liu XX, et al. Polypropylene/montmorillonite composites and their application in hybrid fiber preparation by melt-spinning. J Appl Polym Sci 2004;92(1):552–8.
[47] Giza E, Ito H, Kikutani T, Okui N. Structural control of polyamide 6/clay nanocomposite fibers by in-line drawing process. J Polym Eng 2000;20(6):403–25.
[48] Loo LS, Gleason KK. Investigation of polymer and nanoclay orientation distribution in nylon 6/montmorillonite nanocomposite. Polymer 2004;45(17):5933–9.
[49] Russo P, Acierno D, Di Maio L, Demma G. Thermal and mechanical characterisation of films from nylon 6/EVOH blends. Eur Polym J 1999;35(7):1261–8.
[50] Brus J, Urbanová M, Kelnar I, Kotek J. A solid-state NMR study of structure and segmental dynamics of semicrystalline elastomer-toughened nanocomposites. Macromolecules 2006;39(16):5400–9.
[51] Gonzalez I, Eguiazabal JI, Nazabal J. New clay-reinforced nanocomposites based on a polycarbonate/polycaprolactone blend. Polym Eng Sci 2006;46(7):864–73.
[52] Morgan AB, Harris JD. Effects of organoclay soxhlet extraction on mechanical properties, flammability properties and organoclay dispersion of polypropylene nanocomposites. Polymer 2003;44(8):2313–20.
[53] Fox T. Bulletin of the American Physics Society 1956;1:123.
[54] Hotta S, Paul DR. Nanocomposites formed from linear low density polyethylene and organoclays. Polymer 2004;45(22):7639–54.
[55] Shah RK, Paul DR. Organoclay degradation in melt processed polyethylene nanocomposites. Polymer 2006;47(11):4075–84.
[56] Nassar N, Utracki LA, Kamal MR. Melt intercalation in montmorillonite/polystyrene nanocomposites. Int Polym Proc 2005;20(4):423–31.
[57] Gahleitner M, Kretzschmar B, Van Vliet G, Devaux J, Pospiech D, Bernreitner K, et al. Rheology/morphology interactions in polypropylene/polyamide-6 nanocomposites. Rheol Acta 2006;45(4):322–30.
[58] Huang XY, Lewis S, Brittain WJ, Vaia RA. Synthesis of polycarbonate-layered silicate nanocomposites via cyclic oligomers. Macromolecules 2000;33(6):2000–4.
[59] Bu W, Isayev AI. Prepregs and laminates of polyetherimide-reinforced by a thermotropic LCP. J Appl Polym Sci 1997;65(2):329–40.
[60] Chan H, Leng Y, Gao F. Processing of PC/LCP in situ composites by closed-loop injection moulding. Compos Sci Technol 2002;62:757–65.
[61] Li JX, Silverstein MS, Hilter A, Baer E. Morphology and mechanical properties of fibers from blends of a liquid crystalline polymer and poly(ethylene terephthalate). J Appl Polym Sci 1992;44(9):1531–42.
[62] Cho JW, Paul DR. Nylon 6 nanocomposites by melt compounding. Polymer 2001;42(3):1083–94.
[63] Fornes TD, Yoon PJ, Keskkula H, Paul DR. Nylon 6 nanocomposites: the effect of matrix molecular weight. Polymer 2001;42(25):9929–40.
[64] Fornes TD, Hunter DL, Paul DR. Nylon-6 nanocomposites from alkylammonium-modified clay: the role of alkyl tails on exfoliation. Macromolecules 2004;37(5):1793–8.
[65] Galgali G, Agarwal S, Lele A. Effect of clay orientation on the tensile modulus of polypropylene-nanoclay composites. Polymer 2004;45(17):6059–69.
[66] Dutta D, Weiss RA, He JS. Compatibilization of blends containing thermotropic liquid crystalline polymers with sulfonate ionomers. Polymer 1996;37(3):429–35.
[67] Chang JH, Choi BK, Kim JP, Lee SM, Bang MS. The effect of composition on thermal, mechanical, and morphological properties of thermotropic liquid crystalline polyester with alkyl side-group and polycarbonate blends. Polym Eng Sci 1997;37(9):1564–71.